Journal of Applied Electrochemistry **30**: 1069–1079, 2000.

Dynamic aspects of the electroreduction of chromic acid solutions

E. SORAGNI[1], C. FONTANESI[1], G. BARANI[1] and V. GANZERLI[2]
[1]*Department of Chemistry, University of Modena, Via Campi 183, 41100 Modena, Italy*
[2]*Oleo Component System O.C.S. s.r.l, Via Salvemini 26, 41100 Modena, Italy*

Received 19 May 1999; accepted in revised form 21 March 2000

Key words: chromium, electrodeposition, impedance, oscillating reaction

Abstract

Potentiodynamic and impedance spectroscopy measurements were performed on ARMCO iron, steels (C30, C40, C50), cast iron and graphite electrodes in a bath of industrial composition: CrO_3 250 g dm^{-3}, H_2SO_4 2.5 g dm^{-3}. Attention focused on the electrochemical reactions occurring before the start of the chromium deposition. The electrochemical evidence is markedly affected by the chemical nature of the cathode. This is rationalized by proposing a reaction mechanism involving the formation, depending on the chemical nature of the substrate, of a passive adsorbed film consisting of mixed chromium and iron oxides. Moreover, the proposed overall scheme accounts for the presence of periodic current oscillations observed both in potentiodynamic and potentiostatic curves. In close agreement, impedance spectra show negative loops when measured at the corresponding potentials.

1. Introduction

The study of the electrodeposition of chromium is a topic of great practical interest because (metallic) chromium coatings are used to confer particular mechanical and decorative finishes to metallic parts.

The process has been the subject of a number of papers dealing with the study of the electrochemical behaviour of solutions containing the chromium cation [1–5], followed by Fink's patent proposal [6]. Studies of particular interest concern the deposition of Cr on Pt, and are aimed at rationalising the overall electroreductive mechanism [7, 8]. Particular attention has also been paid to the analysis of some factors which appear to influence this process, namely, the presence in solution of organic species [9, 10], the role of the anions (especially of the halogeno group and SO_4^{2-}) [11, 12], the identification and characterization of intermediate reacting chemical species [13] and the effect of temperature [14, 15]. Recently, there has been renewed interest in the study of this process, primarily due to the need to find a practical alternative to the chromic acid solutions as the main reducible medium, since Cr(VI) compounds are toxic and carcinogenic. Also, some aspects of this process are not properly understood owing to the poor reproducibility of electrochemical data, as observed also in industrial applications.

The aim of this work is to study the role played by the substrate in the chromium electroplating process, with particular reference to the occurrence of current oscillations in the potentiodynamic and potentiostatic curves. The latter phenomenon suggests that the overall electrochemical system is characterized by a complex dynamical behaviour. Accordingly, a series of iron-based substrates (C30, C40, C50 and grey cast iron), frequently used in industrial applications, have been investigated. Tests have also been performed on ARMCO iron (to evaluate the effect of iron carbides, cementite) and on graphite (to ascertain the role played by free carbon in the grey cast iron). Finally, an electroreduction mechanism is proposed, concerning the reactions occurring at more positive potentials (i.e., from −0.50 to −1.00 V vs SCE) than that at the onset of chromium deposition (about −1.10 V vs SCE).

2. Experimental details

Solutions were made following a classical industrial plating bath composition: 250 g dm^{-3} CrO_3 (Aldrich Chem. Co.), 2.5 g dm^{-3} H_2SO_4 (Carlo Erba R. P. E.) in H_2O.

Potentiodynamic (i/E) and chronoamperometric (i/t) curves were recorded using both an Ecochemie PGSTAT 20 and EG&G 710A electrochemical systems, using a 5 mV s^{-1} scan rate.

Impedance spectroscopy measurements were made using the Solartron 1286 electrochemical interface and 1250 frequency response analyser. These latter were driven by an IBM PS2 mod.30 personal computer using an originally developed software.

A three-electrode cell system was used in electrochemical experiments, Figure 1. Working electrode surfaces were prepared by cutting discs from commercial

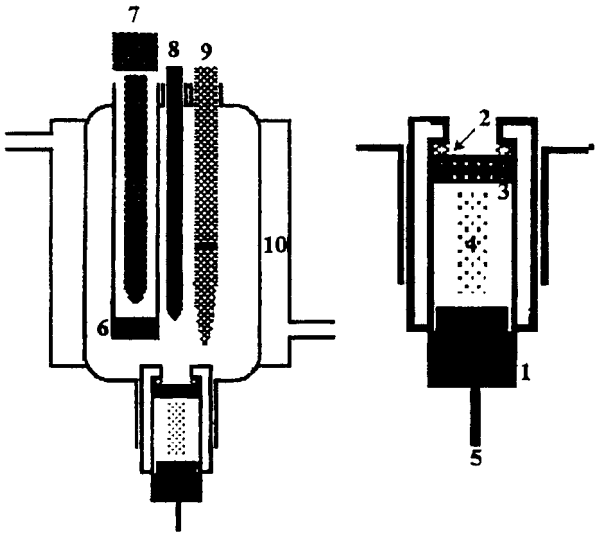

Fig. 1. Cell used on the polarization potentiodynamic curves: (1) Teflon support, (2) trimming, (3) cathode, (4) spring, (5) screw contact, (6) separating septum, (7) anode (Pt), (8) thermometer, (9) reference electrode, (10) thermostatic jacket.

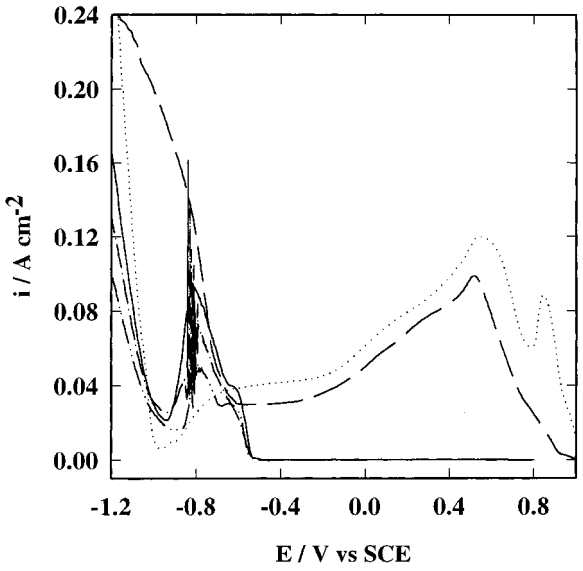

Fig. 2. Direct scan potentiodynamic curves: scan rate 5 mV s^{-1}; CrO_3 250 g dm^{-3}, H_2SO_4 2.5 g dm^{-3}; 50 °C. (———) ARMCO iron, (— · — ·) C40, (— ·· — ··) C50, (— —) Cast iron, (· · · · · ·) graphite.

ARMCO iron, C30, C40, C50 steels and grey cast iron; graphite electrodes were obtained from battery elements. The surfaces were mirror finished using emery papers and Allumina powder paste (AP paste Struers). The exposed surface was 1.0 cm^2. A platinum sheet was used as *counter* electrode. A saturated calomel electrode (SCE) was used as *reference* electrode.

All the potential values reported in this paper are referred to the SCE. All the measurements were carried out at (323 ± 0.1) K.

3. Results and discussion

3.1. *Potentiodynamic results*

Figure 2 sets out potentiodynamic curves (direct scans, from rest potential to −1.2 V), starting from the rest potential and scanning towards potentials typical of the chromium deposition in the case of five different substrates: ARMCO iron, C30, C40 and C50 steels, grey cast iron, graphite. Carbon steels and ARMCO iron potentiodynamic curves are flat from the rest potential, about +0.80 V, up to −0.45 V, then two cathodic peaks are found at −0.65 and −0.80 V, the second of which is sharper and shows a higher current. The peak current density values are inversely proportional to the steel carbon content.

At more negative potentials the current density first decreases to a minimum at −1.00 V and then increases very quickly owing to the onset of the metallic chromium deposition. Oscillations in the current density are present at −0.80 V.

Cast iron exhibits a completely different behaviour: a first broad peak is present at +0.50 V characterized by a rather large current density value (0.09 A cm^{-2}), which decays smoothly until a 'plateau' is attained, 0.03 A cm^{-2}, at potentials between −0.35 and −0.62 V. At more negative potentials the current increases monotonically but a slope change can be observed at −0.80 V.

The graphite potentiodynamic curve indicates that pure carbon present within the pearlitic matrix is responsible for the grey cast iron electrochemical behaviour between +1.03 (rest potential) and −0.65 V. For potentials more negative than −0.65 V, the (i/E) pattern differs from those shown by the other iron alloys. The current density decreases to a minimum at −0.9 V and then increases faster than all the other investigated substrates (with a current density value of 0.28 A cm^{-2} at −1.20 V). All the materials examined show similar current density values at −0.60 V, thus suggesting the occurrence of closely related chemical reactions.

Figure 3 sets out potentiodynamic curves (reverse scans, from −1.2 V to the rest potential). Carbon steels and ARMCO iron do not show a current peak, which is a strong indication of the irreversible nature of the cathodic processes active during the forward scan (Figure 3).

Cast iron and graphite show a slow current decay (Figure 3). The current remains cathodic, with fairly high values, up to very anodic potentials (0.8 V). At 0.80 V the cast iron (i/E) curve has a gentle change of slope (0.075 A cm^{-2}). At the same potential the graphite curve presents a larger current density and oscillations of small amplitude. Both these materials display a broad cathodic peak from 0.0 to +0.80 V, thus ruling out the occurrence of oxidation reactions.

The strong differences observed in the (i/E) curves are a clear indication of the influence of the nature of the substrate on the overall electroreductive process.

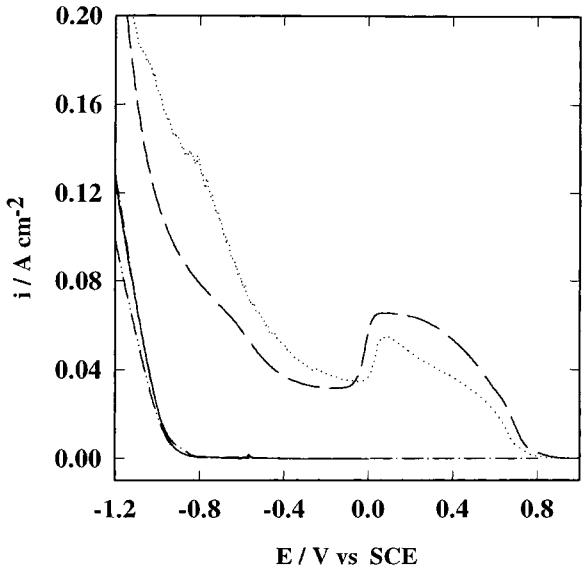

Fig. 3. Reverse scan potentiodynamic curves, same conditions and same symbols as Figure 2.

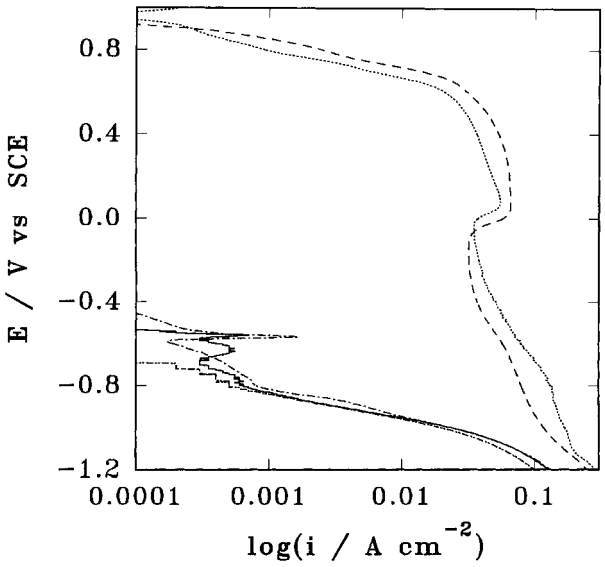

Fig. 5. Semilogarithmic plot of data shown in Figure 3.

3.2. *Tafel analysis*

The data of Figures 2 and 3, transferred into semilogarithmic coordinates (E against $\log(i)$), give the curves of Figures 4 and 5. Assuming the scan rate of 5 mV s^{-1} is slow enough, this kind of plot allows calculation of the Tafel parameters in the potential ranges where a linear relationship is found between E and $\log(i)$. The calculated parameters are recorded in Table 1 (direct scan) and Table 2 (reverse scan) together with the respective potential ranges.

Carbon steels and ARMCO iron reveal the existence of a current peak at positive potentials +0.01 and +0.55 V ($i < 0.001$ A cm^{-2}) Figure 4. The latter corresponds roughly to a current peak (0.1 A cm^{-2}) also present on cast iron at +0.512 V.

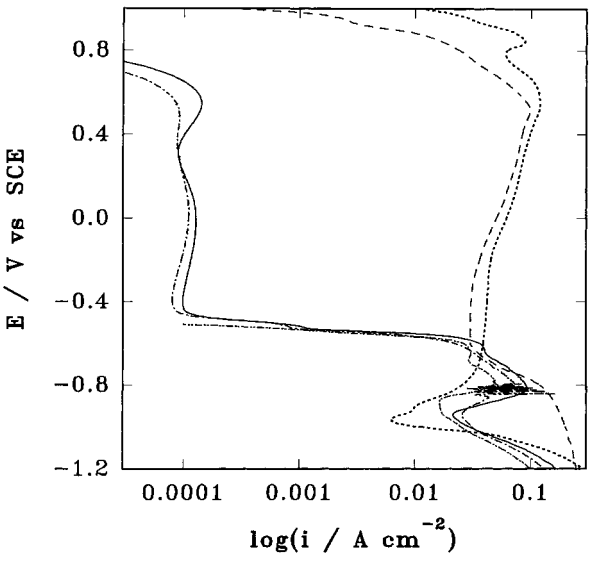

Fig. 4. Semilogarithmic plot of data shown in Figure 2.

First of all, account must be taken of the high positive rest potential assumed by ARMCO iron and carbon steels in chromic acid solution by comparison with that (−0.5 V) of iron in inorganic acid solutions. This noble potential may be regarded as a mixed potential due to the following reactions.
Iron acid corrosion:

$$Fe + H_2Cr_2O_7 \rightarrow FeCr_2O_7 + H_2 \quad (1)$$

Followed by the following partial reactions.
Oxidation:

$$2\,FeCr_2O_7 + 3\,H_2O \rightarrow Fe_2O_3 + 2\,H_2Cr_2O_7 + 2\,H^+ + 2\,e^- \quad (2)$$

Reduction:

$$4\,H_2Cr_2O_7 + 6\,H^+ + 6\,e^- \rightarrow Cr_2(Cr_2O_7)_3 + 7\,H_2O \quad (3)$$

Possible combination reactions:

$$6\,FeCr_2O_7 + 2\,H_2O \rightarrow Cr_2(Cr_2O_7)_3 + 3\,Fe_2O_3 + 2\,H_2Cr_2O_7 \quad (4)$$

or

$$6\,FeCr_2O_7 + 4\,H_2Cr_2O_7 \rightarrow 3\,Fe_2(Cr_2O_7)_3 + Cr_2O_3 + 4\,H_2O \quad (5)$$

The Cr(III)Cr(VI) salt is less stable than the Fe(III)Cr(VI) one [17, 18]. The formation on the iron surface of a chromium oxide film, or of a mixed chromium iron oxide film, is possible and would lead to the passivation of the electrode surface:

$$6\,FeCr_2O_7 + 5\,H_2O \rightarrow 3\,Fe_2O_3 + Cr_2O_3 + 5\,H_2Cr_2O_7 \quad (6)$$

Table 1. Tafel parameters (*a* intercept, *b* slope) calculated for the direct scans

Metal	Potential range 1	–*a*/V	–*b*/V	αn	Potential range 2	–*a*/V	–*b*/V	αn
ARMCO Fe	–0.45/–0.50	0.642	0.043	1.49	–0.96/–1.12	1.326	0.211	0.30
	–0.50/–0.55	0.591	0.019	3.32				
C30	–0.44/–0.48	0.601	0.040	1.58	–0.90/–1.15	1.396	0.277	0.23
	–0.48/–0.52	0.549	0.019	3.32				
C40	–0.45/–0.50	0.642	0.043	1.49	–1.0/–1.15	1.373	0.238	0.27
	–0.50/–0.55	0.617	0.028	2.29				
C50	–0.52/–0.55	0.645	0.038	1.68	–1.02/–1.12	1.550	0.277	0.23
	–0.55/–0.58	0.629	0.030	2.15				
C. Iron	0.80/0.90	–0.861	0.040	1.58	–0.65/–0.71	1.557	0.626	0.10
	0.90/1.00	–0.746	0.070	0.91	–0.71/–0.75	1.139	0.334	0.19
					–0.75/–0.80	0.997	0.224	2.86
Graphite	0.80/0.90	–0.818	0.093	0.69	–0.98/–1.03	1.110	0.055	0.29
	0.90/1.00	–0.729	0.138	0.46	–1.03/–1.12	1.250	0.158	0.40

The standard reduction potentials (vs NHE) of electrochemical reactions leading to some of these solid products are reported in the literature [19]:

$$2\,CrO_2 + 2\,H^+ + 2\,e^- \rightarrow Cr_2O_3 + 2\,H_2O \qquad (E^\circ = 1.06 - 0.059\,pH) \quad (7)$$

$$Cr_2O_7^{2-} + 8\,H^+ + 6\,e^- \rightarrow Cr_2O_3 + 4\,H_2O \qquad (E^\circ = 1.01 - 0.079\,pH - 0.0098\log(Cr_2O_7^{2-})) \quad (8)$$

$$Cr_2O_3 + 6\,H^+ + 6\,e^- \rightarrow 2\,Cr + 3\,H_2O \qquad (E^\circ = -0.579 - 0.059\,pH) \quad (9)$$

$$CrO + 2H^+ + 2\,e^- \rightarrow Cr + H_2O \qquad (E^\circ = -0.588 - 0.059\,pH) \quad (10)$$

These potentials are affected by the presence of complexing agents like sulphuric acid or of organic anions like $HCOO^-$ and ϕCOO^-. All the potentials of the reactions involving solid chromium oxides and metallic chromium have very similar and negative E° values, except that of Cr(IV) → Cr(III) reduction. It should be noted that some of these reactions take place at higher pH values than those measured in chromic acid solutions (<0), thus suggesting that a localized pH increase takes place at the electrode surface/solution interface.

ARMCO iron and steels (between −0.45 and −0.55 V) display a similar E against $\log(i)$ behaviour, each curve being characterized by the presence of two linear patterns separated by an inflection. For potentials more positive with respect to the inflection, the Tafel slope b is almost independent of the nature of the electrode, and the calculated b values are 0.043 V (ARMCO), 0.040 V (C30), 0.043 V (C40), 0.038 V (C50), Table 1. The mean value is 0.041 V and is consistent with a two-electron reaction scheme [20]:

$$A + e^- \rightarrow A^{\cdot -}$$

$$A^{\cdot -} + e^- \rightarrow A^{2-}$$

Or as an alternative:

$$A + e^- \rightarrow A^{\cdot -}$$

$$A^{\cdot -} + A + e^- \rightarrow A_2^{2-}$$

Although the hydrogen evolution process may fit the foregoing reaction scheme, following a Tafel chemical desorption mechanism (slope 0.030 V, 25 °C) [21], it is reasonable to rule out such a process, because the potential is too positive (by about 0.150 V) with respect to −0.75 V, which is the potential value of the hydrogen evolution on iron.

In this case the Tafel slope value obtained (0.04 V) yields $\alpha n \approx 1.5$. Assuming $0.3 < \alpha < 0.7$ (usually considered a

Table 2. Tafel parameters (*a* intercept, *b* slope) calculated for the reverse scans

Metal	Potential range 1	–*a*/V	–*b*/V	αn	Potential range 2	–*a*/V	–*b*/V	αn
ARMCO Fe	–0.82/–0.88	1.242	0.136	0.47	–0.90/–0.96	1.180	0.113	0.57
C30	–0.82/–0.88	1.219	0.129	0.50	–0.90/–0.96	1.179	0.113	0.57
C40	–0.84/–0.86	1.061	0.079	0.81	–0.88/–0.92	1.308	0.179	0.36
C50	–0.82/–0.88	1.209	0.125	0.51	–0.90/–0.96	1.197	0.118	0.54
C. Iron	0.71/0.74	–0.489	0.114	0.56	0.76/0.80	–0.338	0.177	0.37
Graphite	0.66/0.70	–0.398	0.134	0.48	0.80/0.84	–0.294	0.166	0.38

reasonable range for α [22]) n values of 5 and 2 are obtained. The latter n value can be explained with the occurrence of an $\vec{E}C\vec{E}$ mechanism (i.e., electrochemical reduction followed by a fast chemical reaction and again another electrochemical reduction step).

The relevant electrochemical reactions could be the reduction of the passive chromium and iron oxide layer, leading to the uncovering of a new active surface.

For potentials more negative with respect to the inflexion (still between -0.45 and -0.55 V), b is proportional to the carbon content: 0.019 V $\Leftrightarrow \alpha n =$ 3.32 (ARMCO and C30), 0.028 V $\Leftrightarrow \alpha n = 2.29$ (C40), 0.030 V $\Leftrightarrow \alpha n$ 2.15 (C50). If $n \approx 2$, α ranges between 1.7 and 1.1. The following reaction scheme is compatible with these results [22]:

$$O + e = I \quad E_1^\circ$$

$$I + e = R \quad E_2^\circ$$

where the second reaction is the rate determining step (slow) and $E_2^\circ > E_1^\circ$, so that the intermediate species I is not stable. In this case, the electrochemical reactions occur on the free active surface of the metal and their kinetics is affected by the nature of the substrate.

These processes could involve redox couples of various nature, since several reactions (involving species featuring different oxidation states) are possible between iron and chromium [17]:

$$Fe(II) + Cr(VI) \rightarrow Fe(III) + Cr(V)$$

$$Fe(II) + Cr(V) \rightarrow Fe(III) + Cr(IV)$$

$$Fe(II) + Cr(IV) \rightarrow Fe(III) + Cr(III)$$

Or chromium disproportion:

$$Cr(III) + 2\,Cr(VI) \rightarrow 3\,Cr(V)$$

$$Cr(II) + Cr(VI) \rightarrow Cr(III) + Cr(V)$$

$$Cr(II) + Cr(V) \rightarrow Cr(III) + Cr(IV)$$

$$Cr(II) + Cr(V) \rightarrow [Cr(OH)_2Cr]^{4+}$$

It is likely that the kinetics of these reactions is influenced by the chemical and physical state of the surface, thus justifying the broad series of peaks in (i/E) curves and their lack of reproducibility. Between -0.95 and -1.10 V carbon steels and ARMCO iron exhibit Tafel slopes that are not ordered with respect to the substrate chemical composition: $0.24 < b < 0.27$ V, considering $\alpha = 0.3$ the apparent number of exchanged electrons is $n = 1$ and $n = 0.8$, in agreement with data previously obtained [23].

Cast iron shows a rest potential (+1.03 V) close to that of graphite, that is, larger than that of carbon steels. Since this alloy undergoes a fast corrosion process in chromic acid solution, the potential cannot be considered a passive potential but a corrosion potential under anodic control. *Cast iron* does not display minima at positive potentials until -0.65 V. The current then starts to increase monotonically with three different slopes (Figure 4). Only the last one, at -0.80 V, is characterized by a slope value close to that of steels. b is 0.22 V ($\alpha n = 0.28$), and if $\alpha = 0.3$ we have $n = 0.95$. However, the cast iron surface is not blocked, whilst graphite shows a minimum in the same potential range: maybe this result is due to the absence of Fe(II) ions, which could play a catalytic role on the chromate reduction reaction.

A further complication arises from the different dependence on the current density of the hydrogen evolution overvoltage on the phases present in the examined materials (Figure 6) [24]; at low current density, the cementite lamellae, which are nobler than the ferritic matrix, can act as a preferentially cathodic site for the reaction of hydrogen evolution, but, owing to the larger hydrogen overpotential of iron carbide, the role is reversed at larger current densities. Thus, changes in the reaction mechanism could also be induced by variations in the current density.

Even though cast iron contains a higher concentration of iron carbide, its electrochemical behaviour depends mainly on the free carbon content. The hydrogen overvoltage is actually always greater on graphite than on iron.

On graphite the passivating reactions, which imply the presence of iron, cannot take place. The rest potential is of +1.02 V and the graphite electrode is found to be impolarizable with a large exchange current density. The E against $\log(i)$ plot, Figure 4, shows two linear patterns between +1.0 and +0.85 V, the slopes are of -0.093 V ($\alpha n = 0.69$) and -0.138 V ($\alpha n = 0.46$).

Carbon steels and ARMCO iron substrates, show two linear regions in log i against E plots, the first in the

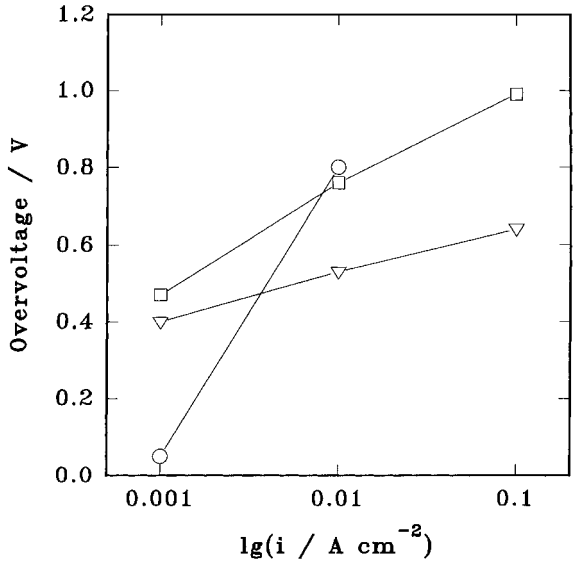

Fig. 6. Hydrogen evolution overvoltage as a function of current density on various compounds: (▽) Fe, (○) Fe_3C, (□) graphite.

potential range between −0.82 and −0.88 V and the second between −0.90 and −0.96 V (Figure 5). Both show a Tafel slope close to 0.120 V, Table 2, indicating that the reaction which occurs in these potential ranges, is mainly hydrogen deadsorption, following the Volmer or Heyrovsky mechanism [20–22].

3.3. *Intermediate species and current oscillations*

Figure 7(a, b, c) shows the results obtained in various measurement sessions, where a single session is carried out performing three consecutive cyclic (i/E) curves, without renewing of the electrode surface (C50 only).

The value of the inversion potential is constant within a single session, and it is selected to evaluate the formation of intermediate reduced compounds: (i) −0.90 V, the potential of the current minimum after the peak at −0.75 V; (ii) −1.00 V, the potential of the onset of chromium deposition; (iii) −1.10 V, a potential where the current has reached a fairly large value; (iv) −1.25 V, massive chromium deposition. 0.0 V is the starting potential, which is common to all the sessions.

Direct scan, Figure 7(a): More negative inversion potentials progressively shift the two current peaks towards more positive potentials. The first peak (the one featuring a more positive potential) disappears as the inversion potential changes from −0.90 to −1.25 V. The second peak is always present even if the current density value decreases steeply as the inversion potential becomes more negative. In the polarization curve up to −1.25 V, a shoulder appears at about −1.00 V. Reverse scans are strictly influenced by the inversion potential and the number of iteration cycles, Figure 7(b) and (c).

Potential reversed at −0.90 V: cycle 1, Figure 7(b), and cycle 3, Figure 7(c), curves are virtually coincident showing a broad peak at −0.65 V followed by a constant current region (centred at −0.40 V).

Potential reversed at −1.00 V: cycle 1, Figure 7(b), and cycle 3, Figure 7(c), curves are similar and three peaks can tentatively be located: −0.65, −0.59, −0.46 V, the first and last could correspond to equivalent peaks found in the −0.90 to 0.00 V curves.

Potential reversed at −1.10 V: cycle 1 and cycle 3 curves are quite different. Cycle 1 shows a sharp desorption peak at −0.70 V followed by a shoulder at −0.65 V. These features are completely lost in cycle 3.

Potential reversed at −1.25 V: cycle 1 and cycle 3 curves are exactly the same: after the sharp current decay following the potential inversion, the curves are flat up to 0.00 V, except for a low peak at −0.55 V.

These results show that the compounds formed at less negative potentials (−0.67 and −0.75 V) are quite stable when they are not reduced at potentials higher than −1.10 V. The splitting of the *i* peak potentials in the *direct* scans (Figure 7(a)), and the appearance of persistent peaks at well-defined potentials (−0.65 and −0.59 V), such as the wide shoulder between −0.50 and −0.35 V, in the backward curves (Figure 7(b) and (c)) can reveal the formation, through fast chemical steps, of compounds of intermediate oxidation state between Cr and Cr(VI). Cr(VI) could also be reduced by atomic hydrogen adsorbed on the iron or chromium crystals: $H_{ADS} + [H_2CrO_4]_{ADS} \rightarrow [H_3CrO_4]_{ADS}$.

This complex situation is reflected by the appearance of current oscillations (ARMCO and carbon steels)

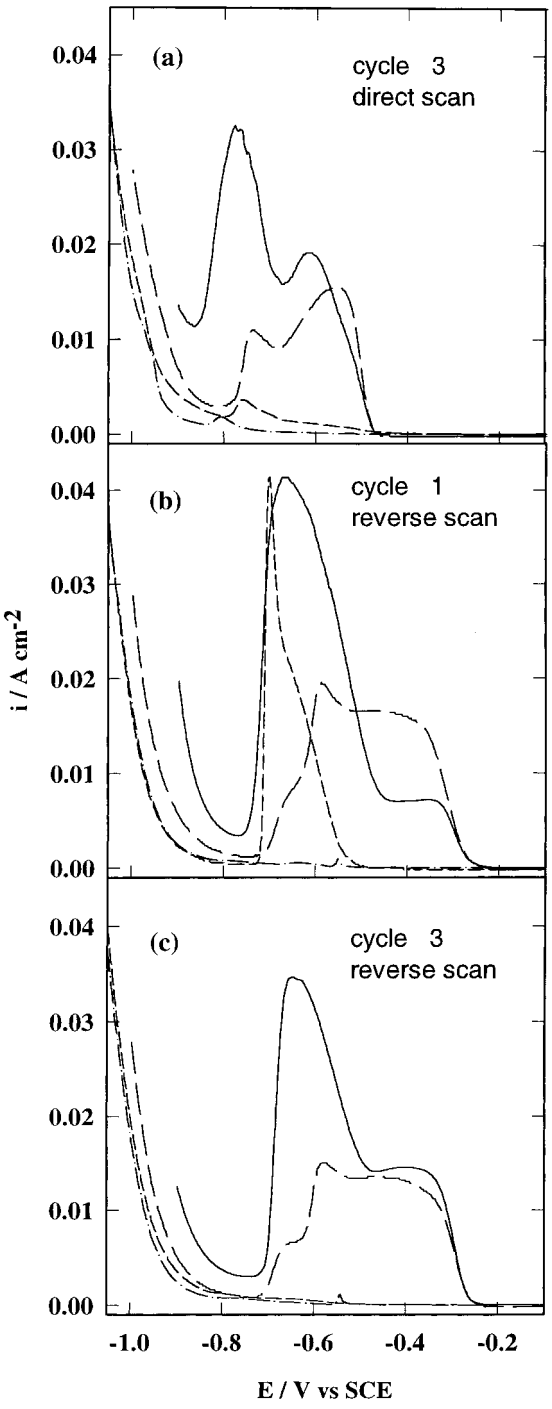

Fig. 7. Potentiodynamic curves (scan rate 5 mV s^{-1}; CrO_3 250 g dm^{-3}, H_2SO_4 2.5 g dm^{-3}; 50 °C) at four inversion potentials: (———) potential range from 0.00 to −0.900 V, (— —) potential range from 0.00 to −1.000 V, (· · · · ·) potential range from 0.00 to −1.100 V and (— · — ·) potential range from 0.00 to −1.250 V vs SCE; (a) direct scan, cycle 3; (b) reverse scan, cycle 1; (c) reverse scan cycle 3.

close to −0.80 V in the potentiodynamic curves, Figure 2. This phenomenon can be rationalized on the basis of the following set of reactions occurring on the electrode surface:

$$3\ Fe^{2+} + HCrO_4^- + 7\ H^+ \rightarrow 3\ Fe^{3+} + Cr^{3+} + 4\ H_2O \quad (11)$$

$$Fe^{3+} + HCrO_4^- = FeCrO_4^+ + H^+ \quad (12)$$

$$FeCrO_4^+ + e^- \rightarrow FeCrO_{4(solid)} \quad (13)$$

$$FeCrO_{4(solid)} + 2\ H^+ \rightarrow H_2CrO_4 + Fe^{2+} \quad (14)$$

The surface can be blocked by the formation of the ferrous chromate (Reaction 13) which, however, is easily soluble in sulphuric acid (Reaction 14), and the active surface is thus restored.

3.4. *Impedance measurements*

Impedance measurements were performed in the −0.55 to −1.1 V range on C50 substrate (Figure 8). The spectra recorded in the −0.50 to −0.77 V range are characterized by the presence of negative loops (i.e., the real part of the impedance (Z_r) is negative and finite when the complex part (Z_i) equals zero [25, 26]). Spectra recorded at −0.78, −0.79, −0.80, −0.85, −0.90 V show two capacitive loops consistent with the simultaneous occurrence of a faradaic reaction and an active adsorption process; the latter can cause the partial passivity of the surface [27–29]. Spectra recorded at −0.95, −1.0, −1.05, −1.10 V show inductive loops consonant with the presence of an active corrosion process.

On the whole, these results appear to agree with findings obtained in the study of the chromium corrosion in H_2SO_4 [30].

Impedance spectra were simulated using the equivalent circuit of Figure 9, where: R_{bulk} is the bulk resistance, C_{dl} the double layer capacitance and R_{ct} the resistance representing the charge transfer reactions; R_{pass} and C_{pass} are, respectively, the resistance and the capacitance of the passivation process, R_b and L_b the resistance and the inductance of the hydrogen blocking and R_{gox} and C_{gox} the resistance and capacitance representing the character change of the passive film; R_{gb} is the dissolution resistance at the grain boundaries and O the finite length diffusion impedance [30]. Table 3 sets out the results of the fitting procedure.

Figure 10 shows the behaviour of the double layer capacity (C_{dl}) and of the charge transfer resistance (R_{CT}) as a function of the applied potential.

C_{dl} is small up to −0.75 V at more negative potentials a larger value is obtained ($\sim 25\ \mu F\ cm^{-2}$) and it decreases again between −0.85 and −0.90 V. This behaviour indicates the possible formation of two adsorbed films of different nature, a result in agreement with the findings obtained by the analysis of potentiodynamic data (see Sections 3.1 and 3.3) and also with the results presented by Saiddington [30]. The higher values in the $-0.75 \leftrightarrow -0.85$ V potential range can be attributed to the start of the hydrogen evolution reaction.

R_{CT} values are negative up to −0.75 V when they abruptly change sign, jumping to a large value which decreases for more negative potentials (probably the onset of the hydrogen evolution, then going towards more negative potentials the R_{CT} values become smaller).

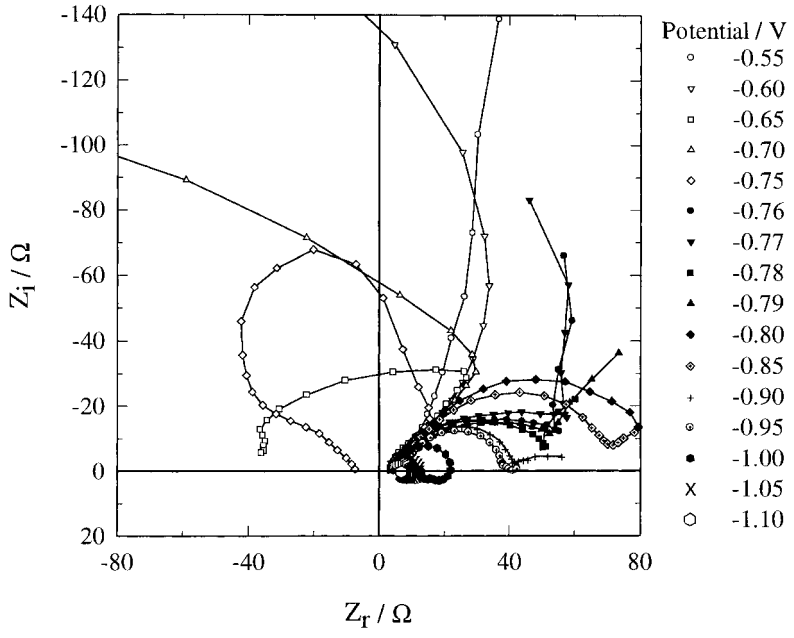

Fig. 8. Impedance spectra.

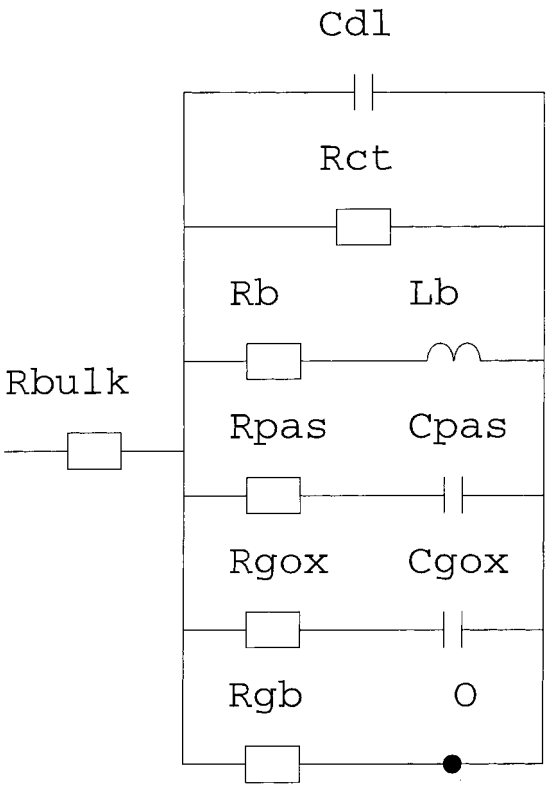

Fig. 9. Equivalent circuit used to fit impedance spectra.

Spectra recorded at potentials more negative than −0.95 V are characterized by the presence of two inductive loops indicating the existence of two simultaneous reactions involving adsorbed species, or more probably a reaction occurring on different sites of the surface, in this case the pearlitic and ferritic areas.

Impedance spectroscopy results were further checked by recording dynamic impedance curves: the real and imaginary part of the impedance are measured at a fixed frequency value, while a linear potential sweep is performed. Figure 11 shows some sample curves recorded at 396, 158, 39 and 10 Hz.

Curves obtained at frequencies higher than 396 Hz are almost coincident. The real and imaginary parts of the impedance are positive and negative, respectively. On the classical complex plane (Z_r against Z_i) these impedance data belong to the high frequency arc locus of points, which is common to all the different potentials selected and representative of the bulk system impedance (Figure 8).

For frequencies lower than 160 Hz the real part Z_r shows a discontinuity at −0.55 V. This discontinuity identifies a vertical asymptote; at the same potential, Z_i displays a large, narrow peak ($Z_i \to -\infty$). Between −0.65 V and −0.75 V Z_r is essentially constant and negative and $Z_i \approx 0$. At $E = -0.75$ V, Z_r crosses back over the zero line and Z_i displays a negative finite peak.

In particular, it should be noted that, Z_r features negative values when Z_i is essentially zero. This finding indicates that the system is close to a bifurcation point,

Table 3. Values obtained fitting the impedance spectra, equivalent circuit of Figure 9

E/V	−0.55	−0.60	−0.65	−0.70	−0.75	−0.76	−0.77	−0.78	−0.79	−0.80	−0.85	−0.90	−0.95	−1.00	−1.05	−1.10
R/Ω	5	5	5.82	6.08	4.94	7	7	8.5	10.30	7	9.97	7.22	9.21	5	4.28	4.35
$C_{dl} \times 10^6$/F	3.58	1.88	2.77	1.39	2.48	24.3	25.4	25.4	29.1	15.0	18.8	34.1	31.6	19.6	15.8	13.1
R_{ct}/Ω	−111.10	−107.57	−5.20	−9.60	145.6	683	236.86	86.26	106.76	143.01	89.39	48.53	32.62	16.41	7.57	5.10
R_{dif}/Ω	74.37	83.52	4.92	7.44	−53.4											
$Y_{dif} \times 10^4$/S	17.0	8.57	229	75.0	604											
$B \times 10^2$/S$^{1/2}$	20.0	4.88	5.22	3.09	20.0											
R_{pas}/Ω	26.98	52.03	34.10	86.22	106.1	47.96	46.72	72.68	62.58	154.72	168.29	109.56	206.78			
$C_{pas} \times 10^6$/F	7.17	7.14	12100	1830	28.4	1820	911	924	686	758	592	1180	160			
R_b/Ω	3468	1534												17.40	3.72	5.71
L_b/H	4.31	159.79												0.326	0.068	0.070
R_{gox}/Ω					17.89											
$C_{gox} \times 10^6$/F					8.30											

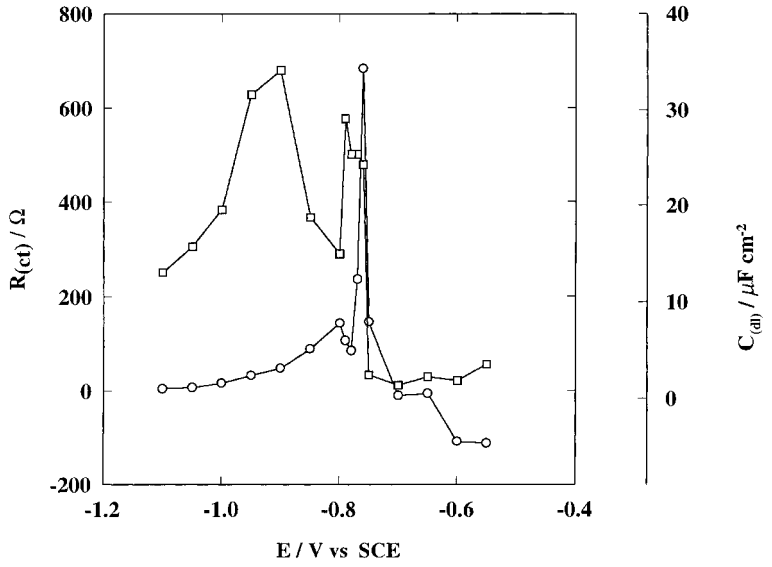

Fig. 10. Plot of double layer capacity, C_{dl} (□), and charge transfer resistance, R_{CT} (○), as a function of applied potential.

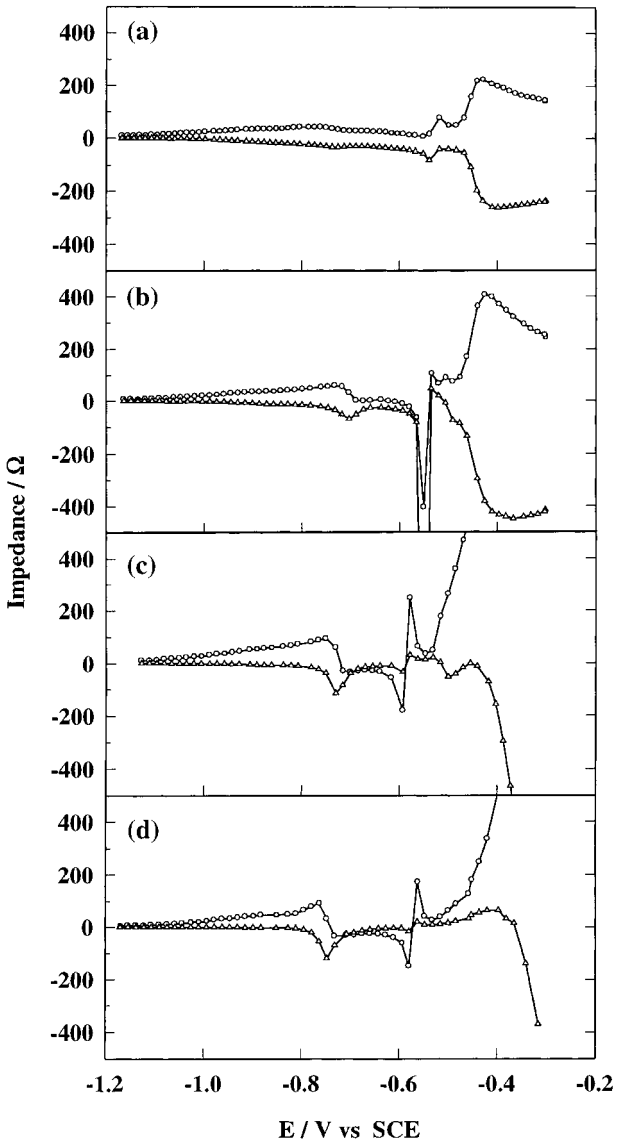

Fig. 11. Dynamic impedance curves: (a) 396 Hz, (b) 158 Hz, (c) 39 Hz, (d) 10 Hz; (○) Z_r, (Δ) Z_i.

in particular to an Hopf bifurcation [24, 25], as: $Z_{(TOT)} = 0$ for $\omega = \omega_H \neq 0$. Thus, a condition of instability can be induced by connecting a resistance in series with the electrochemical cell.

In the potentiodynamic curves of Figure 12, recorded with a resistance in series with the cell, the current densities show periodic oscillations. These oscillations are also present in the current against time curves (Figure 13). Also oscillations of different amplitude are present simultaneously (Figure 14), thus confirming not only the competition of two states (active/passive) but also the fact that the passive state could be due to two different situations (consistent with the formation of two films of different chemical nature [31]).

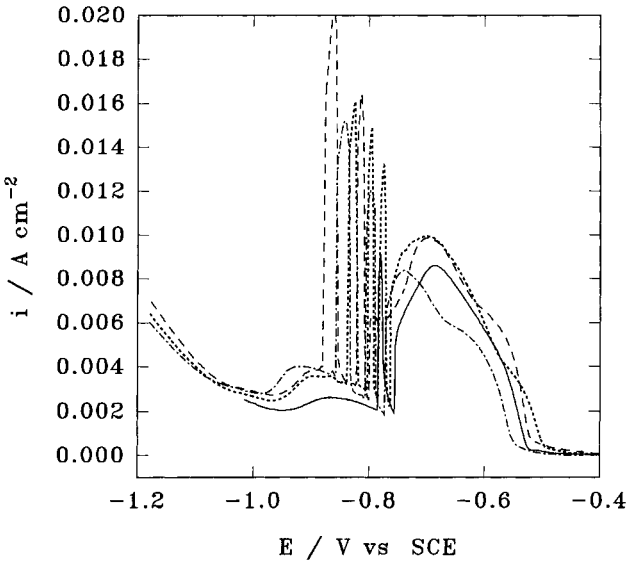

Fig. 12. Potentiodynamic polarisation curves performed with a constant resistance in series to the electrochemical cell: (———) 17 Ω, (— —) 20 Ω, (· · · · · ·) 22 Ω, (— · — ·) 25 Ω.

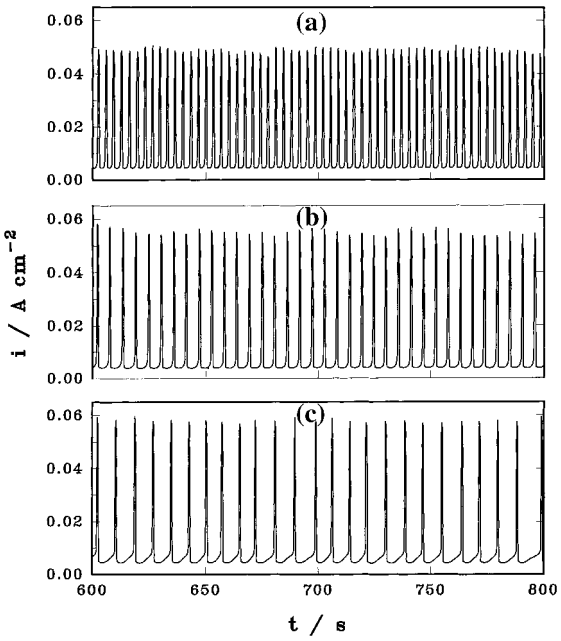

Fig. 13. Chronoamperometric curves at constant potentials: (a) −0.820 V, (b) −0.840 V; (c) −0.860 V.

Upper and lower current limits can be tentatively identified in the potentiodynamic curves (Figure 2), since the amplitude of the oscillations falls within the graphite and cast iron (i/E) curves.

Finally, current time series showing totally uncorrelated oscillations were recorded, Figure 14 which seems to indicate the intrinsic chaotic nature of the chromium electrodeposition reactive system. This last point is currently under investigation in this laboratory.

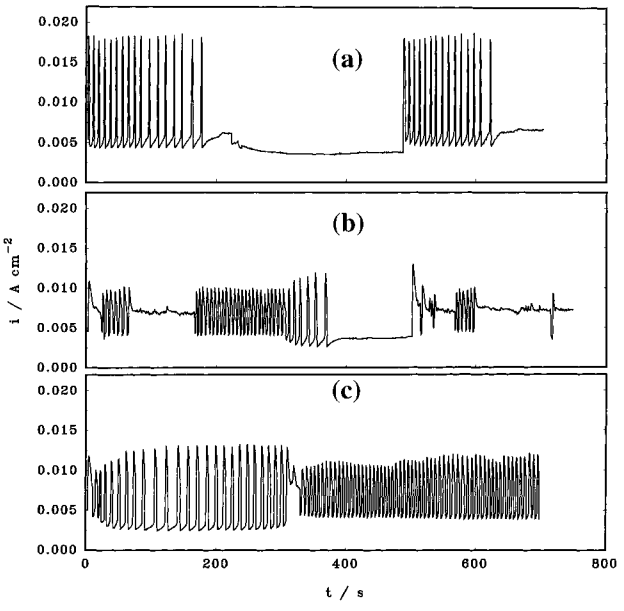

Fig. 14. Chronoamperometric curves at constant potential (−0.840 V) with a fixed resistance in series to the cell: (a) 11 Ω, (b) 19 Ω, (c) 20 Ω.

4. Conclusions

A model of the passive state of steels in chromic/sulphuric acid solutions and the reactions occurring before the start of the electrochemical reduction of Cr(VI) to metallic chromium is proposed. The formation of oxides of mixed Cr valence, also featuring the presence of iron, is shown to be consistent both with our electrochemical results and with the formation of two adsorbed films of different nature, as previously indicated by Saiddington (see [8] and the references cited therein). Impedance measurements also agree with this overall picture in terms of the non-linear complex nature of this system, as witnessed by the presence of negative loops in the impedance spectra.

Acknowledgements

The authors are grateful to the University of Modena and Reggio Emilia for financial support and also to O. C. S. Group s.r.l. for the valuable technical collaboration.

References

1. A. Geuter, *Liebigs Annalen* **99** (1856) 14.
2. G.J. Sargent, *Trans. Am. Soc.* **37** (1920) 479.
3. E. Liebreich, *J. Electrochem. Soc.* **27** (1921) 94, 252; **29** (1923) 208; **33** (1927) 69; **40** (1934) 73.
4. J.P. Hunt and H. Taube, *J. Chem. Phys.* **19** (1951) 602; **18** (1950) 757.
5. G. Dubpernell, *Plating* **47** (1960) 35.
6. C.G. Fink, US Patent 1 581 188 (1926).
7. J.P. Hoare, *J. Electrochem. Soc.* **126** (1979) 190.
8. J.P. Saiddington and G.R. Hoey, *J. Electrochem. Soc.* **117** (1970) 1012.
9. J. McDougall, M. El-Sharif and S. Ma, *J. Appl. Electrochem.* **28** (1998) 929.
10. S.V. Vashchenko and Z.A. Solv'eva, *Russian J. Electrochem.* **30** (1994) 220.
11. J.L. Griffin, *Plating* **53** (1966) 196.
12. Z.A. Solov'eva and L.M. Solodkova, *Elektrokhimyia* **12** (1976) 47.
13. C. Bergenstof Nielsen, P. Leisner and A. Horsewell, *J. Appl. Electrochem.* **28** (1998) 141.
14. C.A. Snavely, *J. Electrochem. Soc.* **92** (1947) 537.
15. L.N. Solodkova and Z.A. Solov'eva, *Elektrokhimiya* **15** (1979) 106.
16. R.A. Anderson and A.S. Kozlovsky, *Am. J. Clin. Nutr.* **41** (1985) 1177.
17. C.L. Rollinson, 'The Chemistry of Chromium, Molybdenum and Tungsten' (Pergamon, Oxford, 1975).
18. G. Bourceanu, V. Melnig, J. Vatamanu and R. Vasiliu, *Electrochim. Acta* **43** (1998) 1031.
19. M. Pourbaix, 'Atlas of Electrochemical Equilibria in Aqueous Solutions' (Pergamon, Oxford/London 1966).
20. M. Noel and K.I. Vasu, 'Cyclic Voltammetry and the frontiers of Electrochemistry', (Aspect Publications, London, 1990).
21. S. Trasatti, *J. Electroanal. Chem.* **39** (1972) 163.
22. P.H. Rieger, 'Electrochemistry' (Chapman & Hall, New York, 1994).
23. E. Soragni, P. Mazzeo and C. Fontanesi, *Mater. Eng.* **8** (1997) 321.
24. G. Wranglen, 'An Introduction to Corrosion and Protection of Metals' (Butler & Tanner, London, 1972).

25. M.T.M. Koper, *Adv. Chem. Phys.* **92** (1996) 161.
26. M.T.M. Koper, *J. Chem. Soc., Faraday Trans.* **94** (1998) 1369.
27. M. Keddam, O.R. Mattos and H. Takenouti, *J. Electrochem. Soc.* **128** (1981) 266.
28. J. Epelboin, C. Gabrielli and H. Takenouti, *Electrochim. Acta* **20** (1975) 913.
29. A.B. Geraldo, O.E. Borcia, O.R. Mattos, F. Huet and B. Tribollet, *Electrochim. Acta* **44** (1998) 455.
30. J.A.L. Dobbelaar and J.H.W. de Wit, J. *Electrochem. Soc.* **137** (1990) 2038.
31. J.P. Saiddington and G.R. Hoey, *J. Electrochem. Soc.* **120** (1973) 1475.